A Shape-Variable, Aqueous, Low-Temperature Liquid Metal–Conductive Polymer Secondary Battery

Hao Fu
School of Materials Science and Engineering, Shaanxi University of Science and Technology
Guicheng Liu (log67@163.com)
Dongguk Univeristy https://orcid.org/0000-0002-3381-1921
Lingyun Xiong
Dongguk Univeristy
Manxiang Wang
Beijing Forestry University
Jeongwoo Lee
Dongguk Univeristy
Ren Ren
Korea Institute of Science and Technology
Woochul Yang
Dongguk University https://orcid.org/0000-0003-3726-2269
Joong Kee Lee
Korea Institute of Science and Technology https://orcid.org/0000-0002-0561-2300

Article

Keywords: liquid metal, GaInSn alloy, aqueous secondary battery, deformability, low-temperature battery.

Posted Date: May 14th, 2021

DOI: https://doi.org/10.21203/rs.3.rs-505283/v1

Version of Record: A version of this preprint was published at Advanced Functional Materials on September 13th, 2021. See the published version at https://doi.org/10.1002/adfm.202107062.

Abstract

A shape-variable aqueous secondary battery operating at low temperature is developed using $Ga_{68}In_{22}Sn_{10}$ in wt% liquid metal anode and conductive polymer (polyaniline (PANI)) cathode. While in the GaInSn alloy anode, Ga is the active constituent; Sn and In increase the acid resistance and decrease the eutectic point to -19°C. This enables the use of strongly acidic aqueous electrolytes (here, pH 0.9), thereby improving the activity and stability of the PANI cathode. Consequently, the battery exhibits remarkable excellent electrochemical performance and mechanical stability. The GaInSn–PANI battery operates via a hybrid mechanism of Ga^{3+} stripping/plating and Cl^- insertion/extraction and delivers a high initial capacity of over 324.6 mAh g^{-1} and a 52.4% retention rate at 0.2 A g^{-1} after 500 cycles, and outstanding power and energy densities of 4300 mW g^{-1} and 98.7 mWh g^{-1}, respectively. Because of the liquid anode, the battery without packaging can be deformed with a small force of several millinewtons without any capacity loss. Moreover, at approximately − 5°C, the battery delivers a capacity of 67.8 mAh g^{-1} at 0.2 A g^{-1} with 100% elasticity. Thus, the battery is promising as a deformable energy device at low temperatures and in demanding environments.

1. Introduction

The rapid growth of smart wearable electronics such as soft robotics[1, 2] and wearable sensors[3–5] has raised the bar on requirements such as elasticity, deformability, low operation temperature, and excellent safety, in addition to flexibility for advanced energy storage devices.[6–15] To achieve flexibility and stretchability with various types of batteries such as Li, Na, Zn, and Al-based batteries, significant efforts have been devoted to replacing the rigid metal-based anodes[16] with flexible electrode materials such as carbon- or metal-based flexible yarn/sheet electrodes,[17–25] spring-structured metal-fiber electrodes with stretchable substrates,[19, 20, 23, 26–28] and liquid metal conductive adhesive-based wearable electrodes.[9, 29–32] Moreover, aqueous batteries are considered promising in terms of safety for wearable devices.[33] Although these studies have achieved remarkable results, solid electrodes have limited stretchability and bendability.[7] In addition, the dendrite growth on solid metal electrode surfaces poses serious safety hazards such as fire and explosion, and is the main bottleneck in battery research.[34, 35] Besides, at sub-zero temperatures, solid electrodes may detach from quasi-solid/solid electrolytes because of the difference in their coefficients of thermal expansion, resulting in the breakdown of the battery circuit.

In contrast to solid electrodes, liquid electrodes offer excellent liquidity and non-dendrite growth.[35, 36] Gallium (Ga)-based liquid metals are considered ideal deformable anodes for wearable aqueous batteries owing to their metallic conductivity, high theoretical capacity (1153.4 mAh g^{-1} for Ga, shown in the Supporting Information), and suitable standard electrode potential (-0.53 V vs $E^{\ominus}$). [6, 30, 37–39] Unlike large-scale stationary liquid metal batteries such as Mg–Sb,[40] Mg–Bi–Sn,[41] and Sb–Pb systems,[42] Ga-based liquid metal batteries with a low eutectic point (< 30°C) obviate the necessity of high working temperatures (> 200°C) and rigorous encapsulation. Although both alkali metal alloys with organic

electrolytes and toxic Hg can be employed as liquid metal electrodes at room temperature,[43] Ga-based alloys which have already been used in wearable electronics,[44–47] are more suitable liquid metal electrodes for the development of wearable aqueous batteries, due to their nontoxicity and high chemical stability in air and aqueous environments.[6] However, a possible drawback with using liquid metals is that a low operating temperature and the stripping/plating of Ga^{3+} may lead to the solidification of a part of the liquid electrode, which leads to poor flexibility and dendritic growth. This can be resolved by employing liquid metals with a wide liquid range at room temperature or a low melting point.

Further, polyaniline (PANI), a classic conductive polymer, has been widely used as a cathode in flexible aqueous batteries, such as flexible Zn–PANI batteries, owing to its high conductivity, stability, and reversible redox reaction in acidic electrolytes.[48, 49] The performance of conductive polymers significantly depends on the acidity of the aqueous electrolyte; that is, the lower the pH, the better are the electrochemical activity and structural stability of the PANI cathode.[50, 51] However, a strong acid may severely corrode the metal anode. Hence, preventing the hydrogen evolution reaction (HER) of metal anodes in strongly acidic electrolytes is a major challenge in aqueous metal–PANI batteries.

In this study, $Ga_{68}In_{22}Sn_{10}$ is used as a liquid metal anode in a shape-variable aqueous liquid metal–PANI secondary battery owing to its high hydrogen evolution potential and low eutectic point. Theoretically, the inert Sn and In can improve the acid resistance of the GaInSn alloy, enabling the use of a highly acidic electrolyte, which in turn improves the activity and stability of the conductive polymer cathode. Moreover, because of a low eutectic temperature (-19°C)[51] and a wide liquid window at room temperature, the GaInSn alloy maintains its liquid phase during the stripping/plating of Ga^{3+}, thereby preventing the detachment of the electrode from the solid electrolyte and imparting flexibility, elasticity, and shape-variability to the liquid metal battery along with a wide operating temperature range. Therefore, the GaInSn–PANI battery with various shapes (one-dimensional (1-D), two-dimensional (2-D), and three-dimensional (3-D) structures) exhibits excellent electrochemical performance with remarkable wearability and deformability even at a sub-zero temperature.

2. Results And Discussion

Flexible liquid metal–polymer batteries assembled with a fluid GaInSn alloy anode, a flexible PANI cathode, and a $GaCl_3/NH_4Cl$/PVA hydrogel electrolyte and encapsulated in an elastic silicone elastomer shell were fabricated as 1-D (fiber), 2-D (sheet) and 3-D (sphere) structures, as shown in Fig. 1a and Supplementary Fig. 1. As illustrated in Fig. 1b–d, the battery pack consisting of 1-D and 3-D batteries connected in series could power a light-emitting diode (LED) either during the stretching and release of the 1-D battery or during various deformations and release of the 3-D battery.

2.1. Effect of Electrolyte Acidity on the Properties of Ga-Based Electrodes

Metal anodes commonly self-corrode due to the HER and acid attack in aqueous electrolytes, especially, [illegible] metal–PANI battery, although the use of a strongly acidic

electrolyte can improve the activity and stability of the PANI cathode, it will aggravate the self-corrosion of the liquid metal anode, resulting in a low open circuit voltage and severe self-discharge.[7, 52] Therefore, the degree of self-corrosion of Ga-based metal anodes in electrolytes with different pH levels was determined by Tafel extrapolation and linear scan voltammetry (LSV), and from the potential distribution during charging and discharging.

The corrosion potentials/rates of Ga, GaIn, and GaInSn as determined from the Tafel curves (Fig. 2a, Supplementary Fig. 2 and Supplementary Table 1) were − 0.87/0.126, -0.82/0.056, and − 0.79 V vs SCE /0.026 mmol per year (mmpy) in the pH 0.9 electrolyte, and − 0.76/0.080, -0.68/0.052, and − 0.65 V vs SCE /0.008 mmpy in the pH 1.6 electrolyte, respectively. The protection efficiencies of GaIn and GaInSn were 16.6% and 79.9% in the pH 0.9 electrolyte, and 31.6% and 94.9% in the pH 1.6 electrolyte, respectively. The result indicates that although the use of the pH 0.9 electrolyte led to more serious metal corrosion than the use of the pH 1.6 electrolyte, the presence of In and Sn in the GaInSn alloy significantly decreased the corrosion rate in each stage in both the electrolytes. The HER of Ga-based metals was measured to determine the nature of metal corrosion. As shown in Fig. 2b, the HER onset potentials of Ga, GaIn, and GaInSn are − 0.71, -0.93, and − 1.09 V *vs* SCE in the pH 0.9 electrolyte, and − 0.93, -1.05, and − 1.15 V *vs* SCE in the pH 1.6 electrolyte, respectively. The result shows that in both electrolytes (pH 0.9 and 1.6), the resistance to the HER increased in the order of Ga < GaIn < GaInSn, since the addition of Sn further increased the resistance of the alloy to the HER because of the high HER overpotentials of In and Sn. To evaluate the effect of electrolyte acidity on the chemical stability of Ga-based metal anodes in the batteries, symmetric cells employing Ga, GaIn, or GaInSn in pH 0.9 and 1.6 electrolytes were tested at a current density of 1.0 mA cm^{-2} for 30 min. As shown in Fig. 2c, the overpotentials of the Ga-based electrodes were higher in the pH 0.9 electrolyte than in the pH 1.6 electrolyte because of the stronger acidity of the former; unlike the GaIn- and Ga-based cells that exhibited unstable charge–discharge voltage curves with large polarizations, the GaInSn-based cell exhibited a stable charge–discharge voltage curve over 150 h with a smaller voltage polarization in both the electrolytes. Therefore, among the Ga-based alloys examined in this study, GaInSn is the most suitable anode candidate for aqueous liquid metal batteries that use a strongly acidic electrolyte.

The cycling performance of the Ga–PANI batteries (Fig. 2d) revealed that the overall performance of the GaInSn-based battery was better in the pH 0.9 electrolyte than in the pH 1.6 electrolyte; the GaInSn-based battery with the pH 0.9 electrolyte exhibited a higher capacity of 252.6 mAh g^{-1} after 500 cycles with a higher average Coulombic efficiency (CE) of 98.6% due to the higher ionic conductivity of the pH 0.9 electrolyte (Supplementary Fig. 3) and high activity of PANI in the strongly acidic electrolyte.[53] In contrast, although the Ga- and GaIn-based batteries exhibited excellent capacities of 496.2 mAh g^{-1} and 473.7 mAh g^{-1} after the first few cycles in the pH 0.9 and pH 1.6 electrolytes, respectively, their capacities significantly decreased to below 50 mAh g^{-1} after 150 cycles because of the low corrosion resistances of Ga and GaIn in the strongly acidic electrolytes, resulting in relatively low CEs (< 89%). Therefore, the GaInSn–PANI battery exhibited the best performance when GaInSn, the most stable alloy, was used as the anode. A comparison of the cycling performances of Ga–PANI, In–PANI, and Sn–PANI batteries

(Supplementary Fig. 4) revealed that due to the chemical inertness of In and Sn, the In- and Sn-based batteries delivered considerably low capacities (< 15 mAh g^{-1}) during the first cycle, which then rapidly decreased to 5 mAh g^{-1}. This indicates that Sn and In are inactive for the battery reactions upon alloying with Ga. Thus, Ga is the only active constituent of the anode in the GaIn–PANI and GaInSn–PANI batteries.

To determine whether the liquid metal anode can stably operate in the acidic electrolytes, anodic and cathodic polarization potential curves were measured from the charge–discharge cycling test. As shown in Fig. 2e and Fig. 2f, after charging, the potentials of the GaIn anode were − 1.26 and − 0.98 V vs SCE, whereas those of the GaInSn anode were − 1.08 and − 1.01 V vs SCE in the pH 0.9 and 1.6 electrolytes, respectively. This, together with the LSV result, (Fig. 2b) indicates that the GaIn anode operates only in the pH 1.6 electrolyte. This is because in the pH 1.6 electrolyte, the anodic potential of GaIn (-0.98 V) is higher than the HER onset potential (-1.05 V), whereas in the pH 0.9 electrolyte, the anodic potential of GaIn (-1.26 V) is much lower than the HER onset potential (-0.93 V); this implies that the HER occurs in the pH 0.9 electrolyte, not in the pH 1.6 electrolyte. In contrast, GaInSn stably operated in both electrolytes as its anodic potential (-1.08 and − 1.01 V, respectively) is higher than the HER onset potentials in both. In the case of the pure Ga anode, a significant portion of the charging curve is below the HER onset potential for both electrolytes (Supplementary Fig. 5), which indicates that Ga is unsuitable as an anode in both electrolytes because of severe corrosion. Moreover, the PANI cathode exhibited a regularly fluctuating cathodic potential in the range of -0.2 to 0.6 V vs SCE during cycling, which avoids structural or morphological damage due to the over-oxidation and over-reduction of PANI.[54, 55] This is essential for the stable performance of the GaInSn–PANI battery and is further confirmed by SEM analysis (Supplementary Fig. 6).

2.2. Working Mechanism of the GaInSn-PANI Battery

The working mechanism of the rechargeable GaInSn–PANI batteries was systematically investigated by scanning electron microscopy (SEM), energy dispersive X-ray spectroscopy (EDS), Raman spectroscopy, and X-ray photoelectron spectroscopy (XPS). As shown in Fig. 3a (Supplementary Fig. 7 and Supplementary Fig. 8), the Ga content of the GaInSn anode decreased from 67.68 wt% to 63.89 wt% after the 1st discharge, increased to 70.96 wt% after the 1st charge, and remained almost unchanged (70.48 wt%) after 100 charging cycles. To accurately evaluate the compositional changes in the anode, the mass fraction, i.e., Ga/Sn and In/Sn ratios (Sn being the most inert metal in the alloy) were determined; the results are shown in Fig. 3b. Because the activities of In and Sn are lower than that of Ga, In/Sn stabilized at approximately 2.07 over 100 cycles, which indicates that Sn and In are the inactive components of the liquid metal anode. In contrast, during charging–discharging, the Ga/Sn ratio (6.427) first decreased to 5.433 and then increased to 7.501, which indicates that Ga is the only active material in the GaInSn anode with the reaction $Ga - 3e^- \rightleftharpoons Ga^{3+}$.[7, 8] Moreover, after 100 charging cycles, the Ga/Sn ratio remained almost constant (with a decrease of 0.52 wt% compared with that after the first charging cycle), which indicates the sufficient reversibility of the proposed anode even after 100 cycles for liquid metal secondary batteries. It is worth noting that the GaIn anode exhibits a similar working mechanism;

however, some small solid In particles appeared on surface of the GaIn anode after discharging (Supplementary Fig. 9b and Supplementary Fig. 10) because the ratio of Ga and In in the GaIn anode exceed the liquid window during stripping (Supplementary Fig. 11). In contrast, even after long-term cycling test, the GaInSn anode still maintained the liquidity due to its wide liquid window (> 55wt% Ga maintain liquidity, shown in phase diagram in Supplementary Fig. 11).

Further, the Raman spectra (Supplementary Fig. 12) exhibited characteristic peaks at 1166.50 and 1480.17 cm^{-1}, which indicate the growth of PANI on the carbon substrate.[56] In addition, the FTIR spectrum of the initial PANI cathode (Fig. 3c) shows peaks around 1493 and 1570 cm^{-1} corresponding to the stretching vibrations of the quinoid diamine ring (N = Q = N) and benzenoid diamine ring (N–B–N), respectively, which imply that the synthesized PANI with the doped = N^+– and un-doped = N– is partially oxidized.[56, 57] And, during the 100 cycles, the N = Q = N and N–B–N signals show a chemical reversibility of PANI in the GaInSn–PANI battery. The XPS profiles of the initial PANI cathode (Fig. 3d) show peaks at 532.7, 399.0, 284.5, and 198.0 eV, which are assigned to O 1s, N 1s, C 1s, and Cl 2p, respectively. During discharge, the N = Q = N signal became more intense, while the N–B–N signal weakened, which is attributed to the reduction of PANI. In detail, after gaining an electron from the anode, the = N^+– and = N– in PANI are reduced to –N– and –N^-–, respectively. Meanwhile, the Cl^- from PANI dissolves into the electrolyte, while Ga^{3+} is embedded into PANI via the reaction between Ga^{3+} and -N^--; this is supported by the disappearance of the Cl^- peak and appearance of a Ga^{3+} peak in the XPS profile. In contrast, after charging, the N = Q = N signal weakened, while the N–B–N signal became intense, indicating the oxidation of PANI; this is confirmed by the reappearance of the Cl signal and disappearance of the Ga signal. The FTIR and XPS results indicate that Cl^- and Ga^{3+}, acting as counter-ions, participate in the redox reactions during the charging and discharging of the GaInSn–PANI battery, as in the case of previously studied Zn–PANI batteries.[58, 59] The cation–anion hybrid mechanism of PANI cathodes has been proposed in previously reported PANI-based batteries with promising performances.[56] In addition, the PANI cathode in the GaIn–PANI battery exhibited the same working mechanism (see the XPS profiles in Supplementary Fig. 13). Therefore, as shown in Fig. 3e, the reaction mechanism of the PANI cathode can be concluded as follows:

$$PANI_{oxd}\text{-}(Cl)_n + (n+3m)e^- + mGa^{3+} \rightleftharpoons (PANI)_{red}\text{-}Ga_m + nCl^- \quad (1)$$

Furthermore, even after 100 cycles, the FTIR spectra remained unchanged and distinct Cl and Ga XPS signals appeared; this confirms the high stability of the PANI cathode in the GaInSn–PANI batteries. In general, during discharging, the Ga atoms that stripped from the GaInSn anode oxidize to form Ga^{3+} in the electrolyte, while the Cl in the PANI cathode reduces to form Cl^-. In contrast, during charging, Cl^- and Ga^{3+} return to PANI and GaInSn, respectively (Fig. 3f). In the charge–discharge process, the Ga from the GaInSn anode and the Cl associated with the PANI cathode act as reversible ions and participate in the redox reaction of the GaInSn–PANI battery. Thus, the overall reaction is as follows:

$$a_m + 1/3n\ Ga^{3+} + nCl^- \quad (2)$$

2.3. Electrochemical Performance of the GaInSn-PANI Battery Under Various Temperatures and Deformability Degrees

The electrochemical performance of the GaInSn–PANI battery in the form of a 2-D sheet was evaluated. As can be seen from the long-term cycling performance (Fig. 4a) and galvanostatic charge/discharge profiles (Supplementary Fig. 14), the GaInSn–PANI battery delivered an initial discharge capacity of approximately 238.2 mAh g^{-1} at 0.2 A g^{-1} with a CE of 58.9%. The capacity increased significantly at the 2nd cycle (343.7 mAh g^{-1}), which is attributed to the activation of the partially oxidized PANI in the initial cycle. After 50 cycles, the capacity significantly decreased to approximately 223.9 mAh g^{-1}, because of the morphological and structural changes in the PANI cathode, and the irreversibly Ga^{3+} trapped in the CF@PANI electrode.[60–62] After 500 cycles at 0.2 A g^{-1}, the GaInSn–PANI battery maintained a reversible capacity of approximately 179.8 mAh g^{-1} with a capacity retention of 80.3% and an average capacity loss of 0.098 mAh g^{-1} $cycle^{-1}$ (Fig. 4a, and Supplementary Table 2). Even at a high current density of 5.0 A g^{-1}, the GaInSn–PANI battery maintained a capacity of 92.8 mAh g^{-1} with a high CE of over 98% and an average capacity loss of 0.013 mAh g^{-1} $cycle^{-1}$ after 500 cycles. This indicates the promising electrochemical performance of the GaInSn–PANI battery at a high current density.

In addition to the outstanding cycling performance, the GaInSn–PANI battery exhibited an excellent rate performance. As shown in Fig. 4b, at low current densities of 0.2, 0.5, and 1.0 A g^{-1}, the battery delivered capacities of 212.1, 168.2, and 134.3 mAh g^{-1}, respectively. At even higher current densities of 2.0 and 5.0 A g^{-1}, the battery delivered capacities of 103.1 and 82.5 mAh g^{-1}, respectively. When the current density reverted to 0.2 A g^{-1}, the capacity recovered to 192.1 mAh g^{-1}, which is comparable to the initial capacity at 0.2 A g^{-1}. Moreover, after 500 cycles, the battery delivered capacities of 196.8, 171.4, and 132.4 mAh g^{-1} at 0.5, 1.0, and 2.0 A g^{-1}, respectively (Supplementary Fig. 15). As can be seen from the Ragone plot (Fig. 4c), the GaInSn–PANI battery exhibits a significantly high energy density of 266.0 mWh g^{-1} with a power density of 217.8 mW g^{-1}. At a high power density of 4300 mW g^{-1}, an energy density of 98.7 mWh g^{-1} was achieved, which are higher than those of existing flexible metal–PANI batteries.[50, 56, 63–66] Further, cyclic voltammetry (CV) was performed at different scan speeds (0.1–1.0 mV s^{-1}) to investigate the electrochemical behaviour of the GaInSn–PANI battery. Figure 4d shows that the area of the CV curves represents the capacity during the electrochemical process. The three peaks at approximately 0.79, 0.95, and 1.10 V indicate the different processes of Ga^{3+}/Cl^{-} reacting with the anode/cathode, and can be used to determine their corresponding capacitive effects according to the equation $i = av^b$, where i (current) and v (scan rate) have a power law relationship.[67] A b value close to 1 indicates a capacitance-controlled process, whereas a b value close to 0.5 indicates a diffusion-controlled process. The b values (slope) can be obtained from the *log i* vs *log v* plot. As shown in Fig. 4e, the b values of the three peaks are 0.81, 0.85, and 0.83, respectively, which indicates that capacitive contribution is the major contribution to total Ga^{3+} storage. The capacitive contribution is further confirmed by the equation $i = k_1v + k_2v^{1/2}$, where k_1v and $k_2v^{1/2}$ are the current contributions of the

 n-controlled process, respectively. By quantification at every

voltage and a certain scan rate, a simulated closed curve was obtained after integration (Fig. 4f). As can be seen, the capacitive process contributes to nearly 68.7% of the total Ga^{3+} storage at a scan rate of 0.6 mV s^{-1}; this suggests that the capacitive process dominates the entire reaction. This is the reason for the high-rate performance and excellent power density of the GaInSn–PANI battery.

Because of the liquid anode, the GaInSn–PANI batteries exhibited excellent cycling performance at low temperatures. As shown in Fig. 4g and Supplementary Fig. 16, the battery delivered capacities of approximately 168.2, 146.6, 103.4, and 64.0 mAh g^{-1} at 25, 15, 5, and − 5°C, respectively, with over 95% CE. The decrease in cycling capacity with decreasing temperature is mainly attributed to the decrease in ion transfer in the poly(vinyl alcohol) (PVA) hydrogels.[68] When the temperature was increased to 25°C, the capacity recovered to 148 mAh g^{-1}. This indicates the good reversibility of the GaInSn–PANI battery at various temperatures.

The mechanical and electrochemical properties of the GaInSn–PANI battery with a 2-D structure in stretched and bent states are shown in Fig. 5. When stretched to 200% (Fig. 5a, Supplementary Fig. 17 and Supplementary Video 1), the battery delivered a capacity (140.9 mAh g^{-1}) comparable to that in the pristine state (142.4 mAh g^{-1}). In addition, the battery exhibited a stable capacity during the bending (bending radius of 5 mm) and recovery processes. The Nyquist plots of the battery in various states are shown in Fig. 5b, and the simulated parameters obtained from the equivalent circuit of $R_e(R_{in}Q_1)(R_{ct}Q_2)W$ (Supplementary Fig. 18) are summarized in Supplementary Table 3 and Supplementary Table 4. The starting point (R_e) reflects the total contact resistance of the batteries, and the first and second arcs correspond to the interfacial resistance (R_{in}) and charge transfer resistance (R_{ct}), respectively. Under the stretched and bent states, the R_{in} of the battery increased by 2–3.5 times and the R_{ct} decreased by 33.7–39.2%, respectively, compared with those of the battery in the pristine state because of the increases in the interface contact area and charge transfer channels between the electrode and electrolyte. Under the combined effect of R_{ct} and R_{in}, the battery exhibited a stable electrochemical performance during bending and stretching.

In addition to the battery-deformation degree mentioned above, the degree of battery-deformation difficulty will also be a necessary factor to be examined for wearable/deformable devices. To quantitatively exhibit the battery-deformation difficulty, the force information was recorded during stretching process. As shown in Fig. 5c, an average force of 0.850 N was required to stretch the battery encapsulated in a rubber shell to 200% of its original length, while almost the same force (0.842 N) was required to stretch the packing shell without the battery to 200% of its original length (Supplementary Fig. 19). This suggests that the battery body without packing requires a force of only several millinewtons (8 and 11 mN for 2-D and 1-D batteries, respectively, as shown in Supplementary Fig. 19 and Supplementary Fig. 20 and Supplementary Video 2) to stretch it to 200% of its original length. This is attributed to the outstanding fluidity of the GaInSn alloy at room temperature, and the special designed electrolyte and PANI cathode. Furthermore, the liquid metal battery demonstrated unique low-temperature

ly stretched to 200% of its original length and recovered its

original state upon release. The results indicate the excellent deformability of the GaInSn–PANI battery at a low temperature, and thus, its promising applicability to flexible devices.

3. Conclusion

A shape-variable and rechargeable aqueous liquid metal–conductive polymer battery operating at low temperature was fabricated using a GaInSn alloy (68 wt% Ga, 22 wt% In, and 10 wt% Sn) anode, PANI cathode, and $GaCl_3$-based hydrogel electrolyte. The anode reaction with Ga as the only active element was ($Ga - 3e^- \rightleftharpoons Ga^{3+}$). And the components of Sn and In enhanced the alloy's acid resistance and decreased the eutectic point to − 19 ^oC, which helped not only to increase the acidity of the aqueous electrolyte to pH = 0.9 to improve activity and stability of PANI cathode, but also to maintain a stable liquid anode at − 5 ^oC. Relatively, due to the hybrid mechanism (the Ga^{3+} stripping/plating and Cl^- insertion/extraction) of PANI, the cathode reaction was $PANI_{oxd}\text{-}(Cl)_n + (n+3m)e^- + mGa^{3+} \rightleftharpoons (PANI)_{red}\text{-}Ga_m + nCl^-$. Therefore, the GaInSn-PANI battery exhibited an excellent performance, with a capacity of 179.8 mAh g^{-1} and a low-capacity decay of 0.098 mAh g^{-1} $cycle^{-1}$ at 0.2 A g^{-1} after 500 cycles. Even at a high current density of 5.0 A g^{-1}, the battery delivered a capacity of 92.8 mAh g^{-1} after 500 cycles. In short, the GaInSn-PANI battery showed more outstanding power and energy densities (98.7 mWh g^{-1} at 4300 mW g^{-1}) compared with other existing stretchable metal-PANI batteries. In addition the satisfying electrochemical performance, because of the liquidity of the liquid metal anode, a force of only several millinewtons was required to deform the 1-D, 2-D, and 3-D batteries without packing, and the batteries could be easily stretched to 200% of their original length, bent to 0.5 cm curvature radius, deformed into various shapes, and recovered their initial state almost without any capacity loss (142.4 mAh g^{-1}). It's worth noting that, the low eutectic temperature leads the battery to an excellent deformation even at -4.6 ^oC with a promising capacity of 64.0 mAh g^{-1}. Although the high molecular weight of liquid metals limits the energy density in weight, the battery still exhibits wide application prospects as a shape-variable soft power source for deep sea mollusk bionic robots as well as in civilian and military fields.

Declarations

Acknowledgements

This work was supported by research grants from the National Research Foundation (Nos. 2019R1C1C1006310, 2020R1I1A1A01072996, 2019H1D3A2A02100593, 2019H1D3A1A01069779, and 2019R1A2C1002844) funded by the government of Republic of Korea, and the KIST Institutional Program (2E30371).

Author Contributions

G.L. and H.F. conceived the idea and designed the experiments. H.F., L.X., J.L., M.W., and R.R. took part in the part of experiments and discussions. H.F. and G.L. prepared the manuscript. G.L., W.Y. and J.K.L. gave

guidance throughout the study and facilitated funding-financial support.

Competing Interest

The authors declare no conflict of interest.

Additional information

Supplementary information is available for this paper at http://doi.org

References

1. Rossiter, J., **Lighting up soft robotics**. *Nat Mater* 2020, *19* (2), **134–135**.
2. Wang, X. L.; Guo, R.; Liu, J., Liquid Metal Based Soft Robotics: Materials, Designs, and Applications. *Adv. Mater.* 2019, *4* (2), 180059.
3. Zhu, M. M.; Lou, M. N.; Abdalla, I.; Yu, J. Y.; Li, Z. L.; Ding, B., Highly shape adaptive fiber based electronic skin for sensitive joint motion monitoring and tactile sensing. *Nano Energy* 2020, *69*, 104429.
4. Ling, Y.; An, T.; Yap, L. W.; Zhu, B.; Gong, S.; Cheng, W., Disruptive, Soft, Wearable Sensors. *Adv. Mater.* 2020, *32* (18), e1904664.
5. Gao, W.; Emaminejad, S.; Nyein, H. Y. Y.; Challa, S.; Chen, K.; Peck, A.; Fahad, H. M.; Ota, H.; Shiraki, H.; Kiriya, D.; Lien, D. H.; Brooks, G. A.; Davis, R. W.; Javey, A., Fully integrated wearable sensor arrays for multiplexed in situ perspiration analysis. *Nature* 2016, *529* (7587), 509–514.
6. Guo, X. L.; Zhang, L. Y.; Ding, Y.; Goodenough, J. B.; Yu, G. H., Room-temperature liquid metal and alloy systems for energy storage applications. *Energy Environ. Sci.* 2019, *12* (9), 2605–2619.
7. Liu, D. Y.; Su, L. S.; Liao, J. H.; Reeja-Jayan, B.; Majidi, C., Rechargeable Soft-Matter EGaIn-MnO2 Battery for Stretchable Electronics. *Adv. Energy Mater.* 2019, *9* (46), 1902798.
8. Liu, G. C.; Kim, J. Y.; Wang, M. X.; Woo, J. Y.; Wang, L.; Zou, D. C.; Lee, J. K., Soft, Highly Elastic, and Discharge-Current-Controllable Eutectic Gallium-Indium Liquid Metal-Air Battery Operated at Room Temperature. *Adv. Energy Mater.* 2018, *8* (16), 1703652.
9. Wu, Y. P.; Huang, L.; Huang, X. K.; Guo, X. R.; Liu, D.; Zheng, D.; Zhang, X. L.; Ren, R.; Qu, D. Y.; Chen, J. H., A room-temperature liquid metal-based self-healing anode for lithium-ion batteries with an ultra-long cycle life. *Energy Environ. Sci.* 2017, *10* (8), 1854–1861.
10. Mackanic, D. G.; Kao, M.; Bao, Z. A., Enabling Deformable and Stretchable Batteries. *Adv. Energy Mater.* 2020, *10* (29), 2001424.
11. Gu, M.; Song, W. J.; Hong, J.; Kim, S. Y.; Shin, T. J.; Kotov, N. A.; Park, S.; Kim, B. S., Stretchable batteries with gradient multilayer conductors. *Sci Adv* **2019**, *5* (7), eaaw1879.
12. Chang, N. N.; Li, T. Y.; Li, R.; Wang, S. N.; Yin, Y. B.; Zhang, H. M.; Li, X. F., An aqueous hybrid electrolyte for low-temperature zinc-based energy storage devices. *Energy Environ. Sci.* 2020, *13* (10), 3527–

13. Nian, Q.; Wang, J.; Liu, S.; Sun, T.; Zheng, S.; Zhang, Y.; Tao, Z.; Chen, J., Aqueous Batteries Operated at -50 degrees C. *Angew. Chem. Int. Ed. Engl.* 2019, *58* (47), 16994–16999.
14. Zhao, Y.; Chen, Z.; Mo, F.; Wang, D.; Guo, Y.; Liu, Z.; Li, X.; Li, Q.; Liang, G.; Zhi, C., Aqueous Rechargeable Metal-Ion Batteries Working at Subzero Temperatures. *Adv. Sci.* 2020, *8* (1), 2002590.
15. Reber, D.; Kuhnel, R. S.; Battaglia, C., Suppressing Crystallization of Water-in-Salt Electrolytes by Asymmetric Anions Enables Low-Temperature Operation of High-Voltage Aqueous Batteries. *ACS Mater. Lett.* 2019, *1* (1), 44–51.
16. Qian, G. Y.; Liao, X. B.; Zhu, Y. X.; Pan, F.; Chen, X.; Yang, Y., Designing Flexible Lithium-Ion Batteries by Structural Engineering. *ACS Energy Lett.* 2019, *4* (3), 690–701.
17. Liu, Q. C.; Xu, J. J.; Xu, D.; Zhang, X. B., Flexible lithium-oxygen battery based on a recoverable cathode. *Nat Commun* 2015, *6*, 7892.
18. Meng, F.; Zhong, H.; Bao, D.; Yan, J.; Zhang, X., In Situ Coupling of Strung Co4N and Intertwined N-C Fibers toward Free-Standing Bifunctional Cathode for Robust, Efficient, and Flexible Zn-Air Batteries. *J. Am. Chem. Soc.* 2016, *138* (32), 10226–10231.
19. Ren, J.; Li, L.; Chen, C.; Chen, X.; Cai, Z.; Qiu, L.; Wang, Y.; Zhu, X.; Peng, H., Twisting carbon nanotube fibers for both wire-shaped micro-supercapacitor and micro-battery. *Adv. Mater.* 2013, *25* (8), 1155–1159.
20. Mo, F.; Liang, G.; Huang, Z.; Li, H.; Wang, D.; Zhi, C., An Overview of Fiber-Shaped Batteries with a Focus on Multifunctionality, Scalability, and Technical Difficulties. *Adv. Mater.* 2020, *32* (5), e1902151.
21. Yu, X.; Fu, Y. P.; Cai, X.; Kafafy, H.; Wu, H. W.; Peng, M.; Hou, S. C.; Lv, Z. B.; Ye, S. Y.; Zou, D. C., Flexible fiber-type zinc-carbon battery based on carbon fiber electrodes. *Nano Energy* 2013, *2* (6), 1242–1248.
22. Chi, S. S.; Qi, X. G.; Hu, Y. S.; Fan, L. Z., 3D Flexible Carbon Felt Host for Highly Stable Sodium Metal Anodes. *Adv. Energy Mater.* 2018, *8* (15), 1702764.
23. Xu, N. N.; Zhang, Y. X.; Wang, M.; Fan, X. J.; Zhang, T.; Peng, L. W.; Zhou, X. D.; Qiao, J. L., High-performing rechargeable/flexible zinc-air batteries by coordinated hierarchical Bi-metallic electrocatalyst and heterostructure anion exchange membrane. *Nano Energy* 2019, *65*, 104021.
24. Gaikwad, A. M.; Zamarayeva, A. M.; Rousseau, J.; Chu, H.; Derin, I.; Steingart, D. A., Highly stretchable alkaline batteries based on an embedded conductive fabric. *Adv. Mater.* 2012, *24* (37), 5071–5076.
25. Chen, W.; Zhang, X.; Mi, L.; Liu, C.; Zhang, J.; Cui, S.; Feng, X.; Cao, Y.; Shen, C., High-Performance Flexible Freestanding Anode with Hierarchical 3D Carbon-Networks/Fe7 S8 /Graphene for Applicable Sodium-Ion Batteries. *Adv. Mater.* 2019, *31* (8), e1806664.
26. Pan, S. W.; Zhang, Z. T.; Weng, W.; Lin, H. J.; Yang, Z. B.; Peng, H. S., Miniature wire-shaped solar cells, electrochemical capacitors and lithium-ion batteries. *Mater. Today* 2014, *17* (6), 276–284.
27. Liu, K.; Kong, B.; Liu, W.; Sun, Y. M.; Song, M. S.; Chen, J.; Liu, Y. Y.; Lin, D. C.; Pei, A.; Cui, Y., Stretchable Lithium Metal Anode with Improved Mechanical and Electrochemical Cycling Stability. *Joule* 2018, *2* (9), 1857–1865.

28. Xu, Y.; Zhao, Y.; Ren, J.; Zhang, Y.; Peng, H., An All-Solid-State Fiber-Shaped Aluminum-Air Battery with Flexibility, Stretchability, and High Electrochemical Performance. *Angew. Chem. Int. Ed. Engl.* 2016, *55* (28), 7979–7982.
29. Kim, M. G.; Lee, B.; Li, M.; Noda, S.; Kim, C.; Kim, J.; Song, W. J.; Lee, S. W.; Brand, O., All-Soft Supercapacitors Based on Liquid Metal Electrodes with Integrated Functionalized Carbon Nanotubes. *Acs Nano* 2020, *14* (5), 5659–5667.
30. Park, S.; Thangavel, G.; Parida, K.; Li, S.; Lee, P. S., A Stretchable and Self-Healing Energy Storage Device Based on Mechanically and Electrically Restorative Liquid-Metal Particles and Carboxylated Polyurethane Composites. *Adv. Mater.* 2019, *31* (1), e1805536.
31. Guo, X. L.; Ding, Y.; Xue, L. G.; Zhang, L. Y.; Zhang, C. K.; Goodenough, J. B.; Yu, G. H., A Self-Healing Room-Temperature Liquid-Metal Anode for Alkali-Ion Batteries. *Adv. Funct. Mater.* 2018, *28* (46), 201804649.
32. Zhu, J. H.; Wu, Y. P.; Huang, X. K.; Huang, L.; Cao, M. Y.; Song, G. Q.; Guo, X. R.; Sui, X. Y.; Ren, R.; Chen, J. H., Self-healing liquid metal nanoparticles encapsulated in hollow carbon fibers as a free-standing anode for lithium-ion batteries. *Nano Energy* 2019, *62*, 883–889.
33. Chao, D.; Zhou, W.; Xie, F.; Ye, C.; Li, H.; Jaroniec, M.; Qiao, S. Z., Roadmap for advanced aqueous batteries: From design of materials to applications. *Sci Adv* 2020, *6* (21), eaba4098.
34. Rahmanifar, M. S.; Mousavi, M. F.; Shamsipur, M.; Ghaemi, M., What is the limiting factor of the cycle-life of Zn–polyaniline rechargeable batteries? *J. Power Sources* 2004, *132* (1–2), 296–301.
35. Ding, Y.; Guo, X.; Qian, Y.; Xue, L.; Dolocan, A.; Yu, G., Room-Temperature All-Liquid-Metal Batteries Based on Fusible Alloys with Regulated Interfacial Chemistry and Wetting. *Adv. Mater.* 2020, *32* (30), e2002577.
36. Ding, Y.; Guo, X.; Yu, G., Next-Generation Liquid Metal Batteries Based on the Chemistry of Fusible Alloys. *ACS Cent Sci* 2020, *6* (8), 1355–1366.
37. Song, W. J.; Kong, M.; Cho, S.; Lee, S.; Kwon, J.; Son, H. B.; Song, J. H.; Lee, D. G.; Song, G.; Lee, S. Y.; Jung, S.; Park, S.; Jeong, U., Stand-Alone Intrinsically Stretchable Electronic Device Platform Powered by Stretchable Rechargeable Battery. *Adv. Funct. Mater.* 2020, *30* (50), 202003608.
38. Kim, H.; Boysen, D. A.; Newhouse, J. M.; Spatocco, B. L.; Chung, B.; Burke, P. J.; Bradwell, D. J.; Jiang, K.; Tomaszowska, A. A.; Wang, K.; Wei, W.; Ortiz, L. A.; Barriga, S. A.; Poizeau, S. M.; Sadoway, D. R., Liquid metal batteries: past, present, and future. *Chem. Rev.* 2013, *113* (3), 2075–2099.
39. Mackanic, D. G.; Chang, T. H.; Huang, Z.; Cui, Y.; Bao, Z., Stretchable electrochemical energy storage devices. *Chem. Soc. Rev.* 2020, *49* (13), 4466–4495.
40. Bradwell, D. J.; Kim, H.; Sirk, A. H.; Sadoway, D. R., Magnesium-antimony liquid metal battery for stationary energy storage. *J. Am. Chem. Soc.* 2012, *134* (4), 1895–1897.
41. Zhao, W.; Li, P.; Liu, Z. W.; He, D. L.; Han, K.; Zhao, H. L.; Qu, X. H., High-Performance Antimony-Bismuth-Tin Positive Electrode for Liquid Metal Battery. *Chem. Mater.* 2018, *30* (24), 8739–8746.
42. Ouchi, T.; Sadoway, D. R., Positive current collector for Li parallel to Sb-Pb liquid metal battery. *J.*

43. Baclig, A. C.; McConohy, G.; Poletayev, A.; Michelson, A.; Kong, N.; Lee, J. H.; Chueh, W. C.; Rugolo, J., High-Voltage, Room-Temperature Liquid Metal Flow Battery Enabled by Na-K vertical bar K-beta "-Alumina Stability. *Joule* **2018**, *2* (7), 1287–1296.
44. Silva, C. A.; Lv, J.; Yin, L.; Jeerapan, I.; Innocenzi, G.; Soto, F.; Ha, Y. G.; Wang, J., Liquid Metal Based Island-Bridge Architectures for All Printed Stretchable Electrochemical Devices. *Adv. Funct. Mater.* 2020, *30* (30), 202002041.
45. Zhu, S.; So, J. H.; Mays, R.; Desai, S.; Barnes, W. R.; Pourdeyhimi, B.; Dickey, M. D., Ultrastretchable Fibers with Metallic Conductivity Using a Liquid Metal Alloy Core. *Adv. Funct. Mater.* 2013, *23* (18), 2308–2314.
46. Bartlett, M. D.; Fassler, A.; Kazem, N.; Markvicka, E. J.; Mandal, P.; Majidi, C., Stretchable, High-k Dielectric Elastomers through Liquid-Metal Inclusions. *Adv. Mater.* 2016, *28* (19), 3726–3731.
47. Chen, S.; Wang, H.-Z.; Zhao, R.-Q.; Rao, W.; Liu, J., Liquid Metal Composites. *Matter* 2020, *2* (6), 1446–1480.
48. Yu, H.; Liu, G.; Wang, M.; Ren, R.; Shim, G.; Kim, J. Y.; Tran, M. X.; Byun, D.; Lee, J. K., Plasma-Assisted Surface Modification on the Electrode Interface for Flexible Fiber-Shaped Zn-Polyaniline Batteries. *ACS Appl Mater Interfaces* **2020**, *12* (5), 5820–5830.
49. Li, X.; Tang, Y.; Lv, H.; Wang, W.; Mo, F.; Liang, G.; Zhi, C.; Li, H., Recent advances in flexible aqueous zinc-based rechargeable batteries. *Nanoscale* 2019, *11* (39), 17992–18008.
50. Shi, H. Y.; Ye, Y. J.; Liu, K.; Song, Y.; Sun, X., A Long-Cycle-Life Self-Doped Polyaniline Cathode for Rechargeable Aqueous Zinc Batteries. *Angew. Chem. Int. Ed. Engl.* 2018, *57* (50), 16359–16363.
51. Liu, T. Y.; Sen, P.; Kim, C. J. C. J., Characterization of Nontoxic Liquid-Metal Alloy Galinstan for Applications in Microdevices. *J Microelectromech S* 2012, *21* (2), 443–450.
52. Lee, S. M.; Kim, Y. J.; Eom, S. W.; Choi, N. S.; Kim, K. W.; Cho, S. B., Improvement in self-discharge of Zn anode by applying surface modification for Zn-air batteries with high energy density. *J. Power Sources* 2013, *227*, 177–184.
53. McManus, P. M.; Cushman, R. J.; Yang, S. C., Influence of oxidation and protonation on the electrical conductivity of polyaniline. *J. Phys. Chem.* 1987, *91* (3), 744–747.
54. Malinauskas, A.; Holze, R., In situ UV-vis spectroelectrochemical study of polyaniline degradation. *J. Appl. Polym. Sci.* 1999, *73* (2), 287–294.
55. Mazeikiene, R.; Malinauskas, A., Kinetic study of the electrochemical degradation of polyaniline. *Synth. Met.* 2001, *123* (2), 349–354.
56. Wan, F.; Zhang, L. L.; Wang, X. Y.; Bi, S. S.; Niu, Z. Q.; Chen, J., An Aqueous Rechargeable Zinc-Organic Battery with Hybrid Mechanism. *Adv. Funct. Mater.* 2018, *28* (45), 201804975.
57. Tang, S. J.; Lin, K. Y.; Zhu, Y. R.; Huang, H. Y.; Ji, W. F.; Yang, C. C.; Chao, Y. C.; Yeh, J. M.; Chiu, K. C., Structural and electrical characterization of polyanilines synthesized from chemical oxidative polymerization via doping/de-doping/re-doping processes. *J Phys D Appl Phys* 2013, *46* (50), 505301.

58. Shim, G.; Tran, M. X.; Liu, G.; Byun, D.; Lee, J. K., Flexible, fiber-shaped, quasi-solid-state Zn-polyaniline batteries with methanesulfonic acid-doped aqueous gel electrolyte. *Energy Storage Mater.* 2021, *35*, 739–749.
59. Mu, S. L.; Shi, Q. F., Controllable preparation of poly(aniline-co-5-aminosalicylic acid) nanowires for rechargeable batteries. *Synth. Met.* 2016, *221*, 8–14.
60. Deng, J. X.; Wang, T. M.; Guo, J. S.; Liu, P., Electrochemical capacity fading of polyaniline electrode in supercapacitor: An XPS analysis. *Prog Nat Sci-Mater* **2017**, *27* (2), 257–260.
61. Zhu, Z. Z.; Wang, G. C.; Sun, M. Q.; Li, X. W.; Li, C. Z., Fabrication and electrochemical characterization of polyaniline nanorods modified with sulfonated carbon nanotubes for supercapacitor applications. *Electrochim. Acta* 2011, *56* (3), 1366–1372.
62. Yu, H. T.; Ge, X.; Bulin, C.; Xing, R. G.; Li, R. H.; Xin, G. X.; Zhang, B. W., Facile fabrication and energy storage analysis of graphene/PANI paper electrodes for supercapacitor application. *Electrochim. Acta* 2017, *253*, 239–247.
63. Yao, H.; Li, Q. J.; Zhang, M. S.; Tao, Z. R.; Yang, Y. Y., Prolonging the cycle life of zinc-ion battery by introduction of [Fe(CN)(6)](4-) to PANI via a simple and scalable synthetic method. *Chem. Eng. J.* 2020, *392*, 123653.
64. Chen, C. X.; Gan, Z. Y.; Xu, C.; Lu, L.; Liu, Y. Q.; Gao, Y. H., Electrosynthesis of poly(aniline-co-azure B) for aqueous rechargeable zinc-conducting polymer batteries. *Electrochim. Acta* 2017, *252*, 226–234.
65. Dong, H.; Liang, Y. L.; Tutusaus, O.; Mohtadi, R.; Zhang, Y.; Hao, F.; Yao, Y., Directing Mg-Storage Chemistry in Organic Polymers toward High-Energy Mg Batteries. *Joule* 2019, *3* (3), 782–793.
66. Soundharrajan, V.; Sambandam, B.; Kim, S.; Mathew, V.; Jo, J.; Kim, S.; Lee, J.; Islam, S.; Kim, K.; Sun, Y. K.; Kim, J., Aqueous Magnesium Zinc Hybrid Battery: An Advanced High-Voltage and High-Energy $MgMn_2O_4$ Cathode. *ACS Energy Lett.* 2018, *3* (8), 1998–2004.
67. Fu, H.; Xu, Z. W.; Li, R. Z.; Guan, W. W.; Yao, K.; Huang, J. F.; Yang, J.; Shen, X. T., Network Carbon with Macropores from Apple Pomace for Stable and High Areal Capacity of Sodium Storage. *ACS Sustain. Chem. Eng.* 2018, *6* (11), 14751–14758.
68. Liu, Y.; Geever, L. M.; Kennedy, J. E.; Higginbotham, C. L.; Cahill, P. A.; McGuinness, G. B., Thermal behavior and mechanical properties of physically crosslinked PVA/Gelatin hydrogels. *J Mech Behav Biomed Mater* 2010, *3* (2), 203–209.

Figures

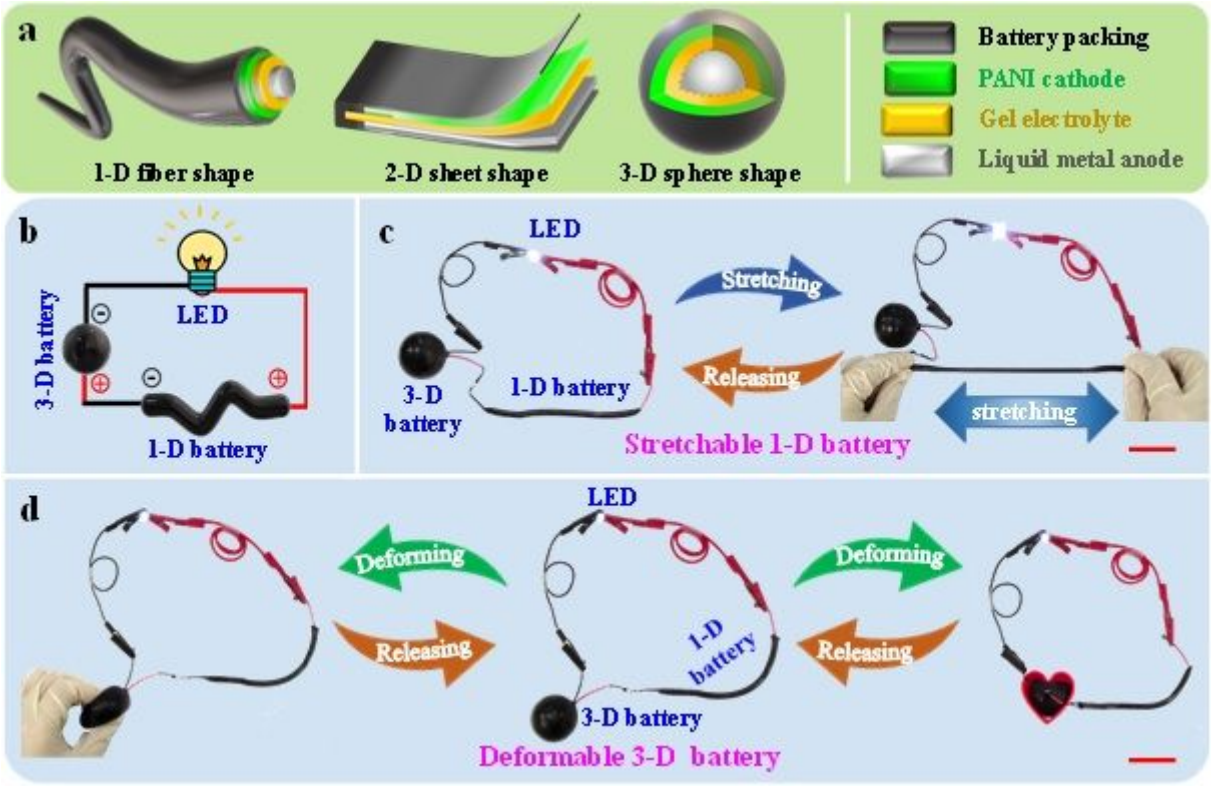

Figure 1

Schematic diagrams and photos of the proposed shape-variable, aqueous liquid metal–conductive polymer secondary batteries. a Schematic of the internal structure of the GaInSn liquid metal–PANI battery with 1-D fiber, 2-D sheet, and 3-D spherical shapes. b Schematic and c, d photos of the LED circuit powered by 1-D and 3-D GaInSn–PANI batteries in stretched, deformed, and released states. The scale red-bars represent 3 cm.

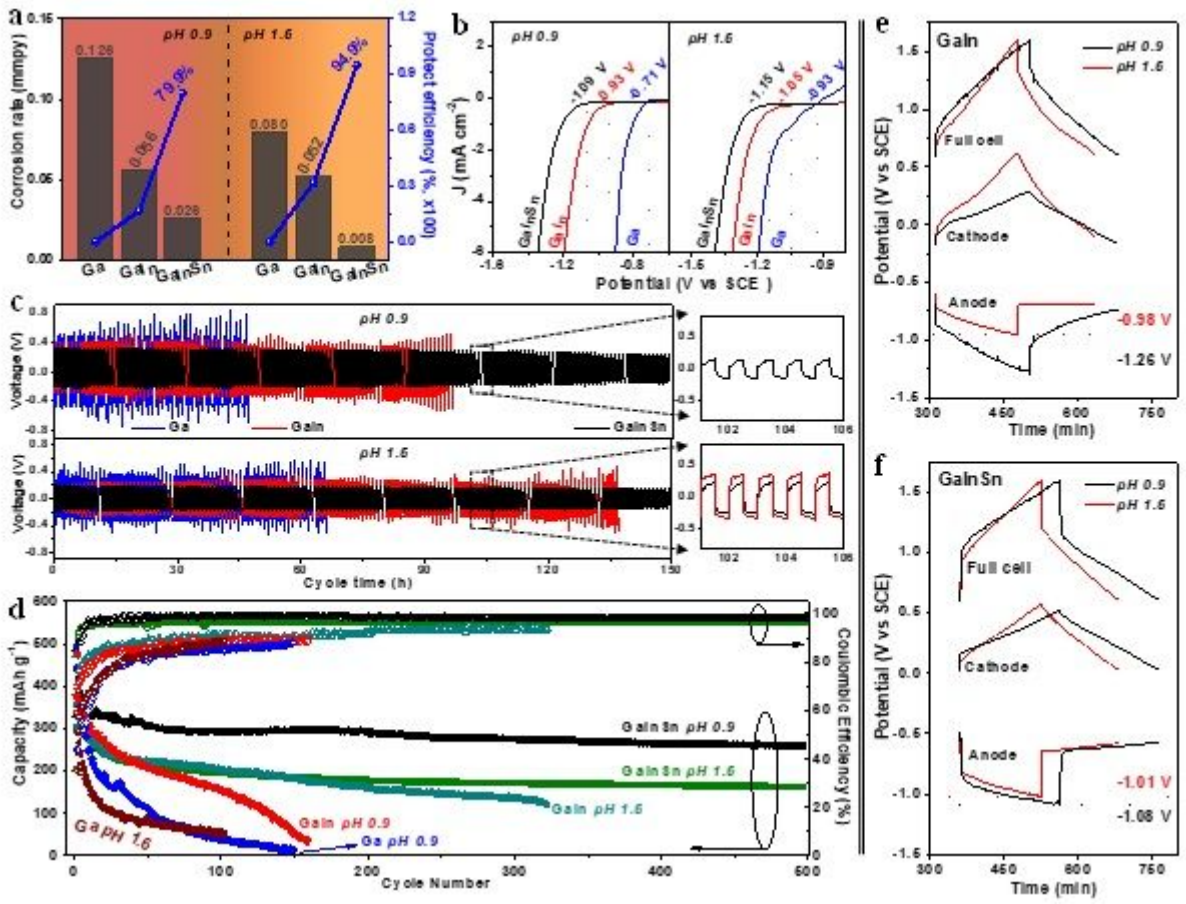

Figure 2

Effect of electrolyte acidity on the physicochemical properties of Ga-based electrodes and batteries. a Corrosion rate and protection efficiency calculated from Tafel plots, b LSV curves, and c symmetric cell test of Ga, GaIn, and GaInSn electrodes in pH 0.9 and 1.6 electrolytes. d Cycling properties of Ga-based metal–PANI batteries in pH 0.9 and 1.6 electrolytes at 0.1 A g-1. Polarization curves of anode, cathode, and battery based on e GaIn and f GaInSn alloys.

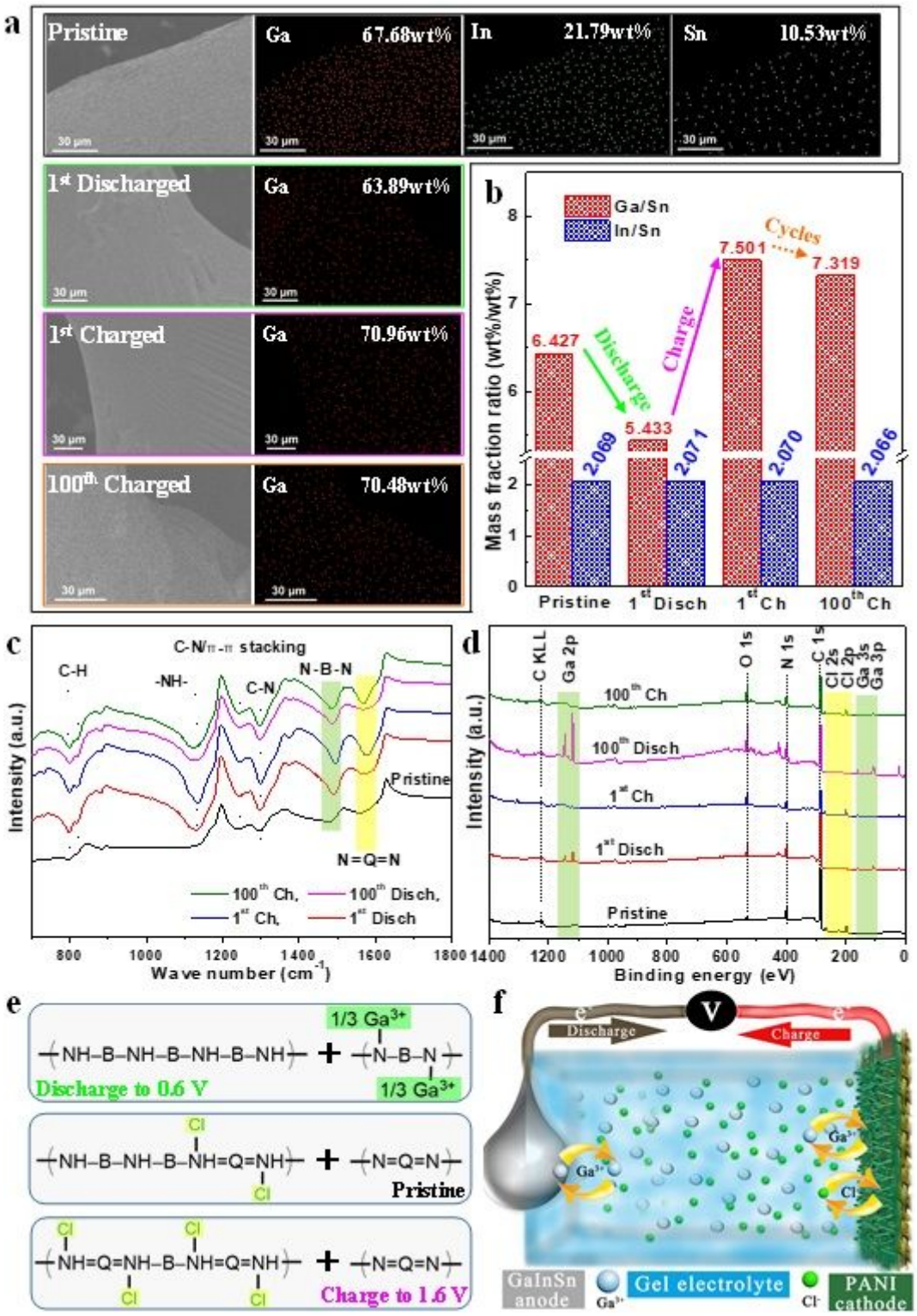

Figure 3

Working mechanism of the GaInSn–PANI battery. Under different cycling states in the pH 0.9 electrolyte (black line in Figure 2d), a EDS mapping images and b mass fraction ratios (i.e. Ga/Sn and In/Sn ratios) of GaInSn anode; c FTIR spectra and d XPS profiles of PANI cathode. Schematic of the proposed reaction mechanisms of e PANI cathode and f GaInSn–PANI battery.

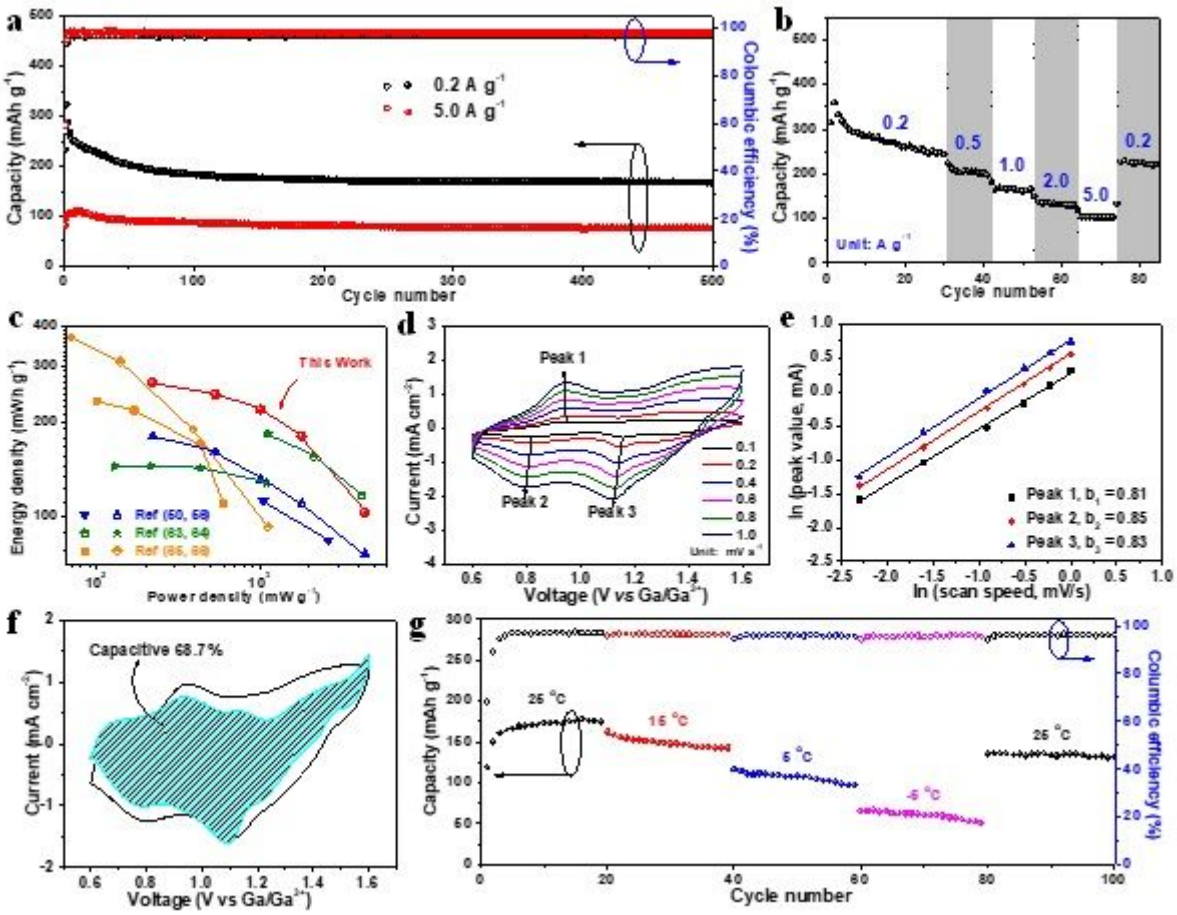

Figure 4

Electrochemical performance of the GaInSn–PANI battery at various current densities and operating temperatures. a Long-term cycling performance at 0.2 and 5.0 A g−1, b rate capabilities, c Ragone plot for comparison with other aqueous PANI batteries, d CV curves at various scan rates, e b values of different redox peaks in the CV plots, f k1 analysis at 0.6 mV s−1, and g cycling performance at 1.0 A g−1 at various operating temperatures.

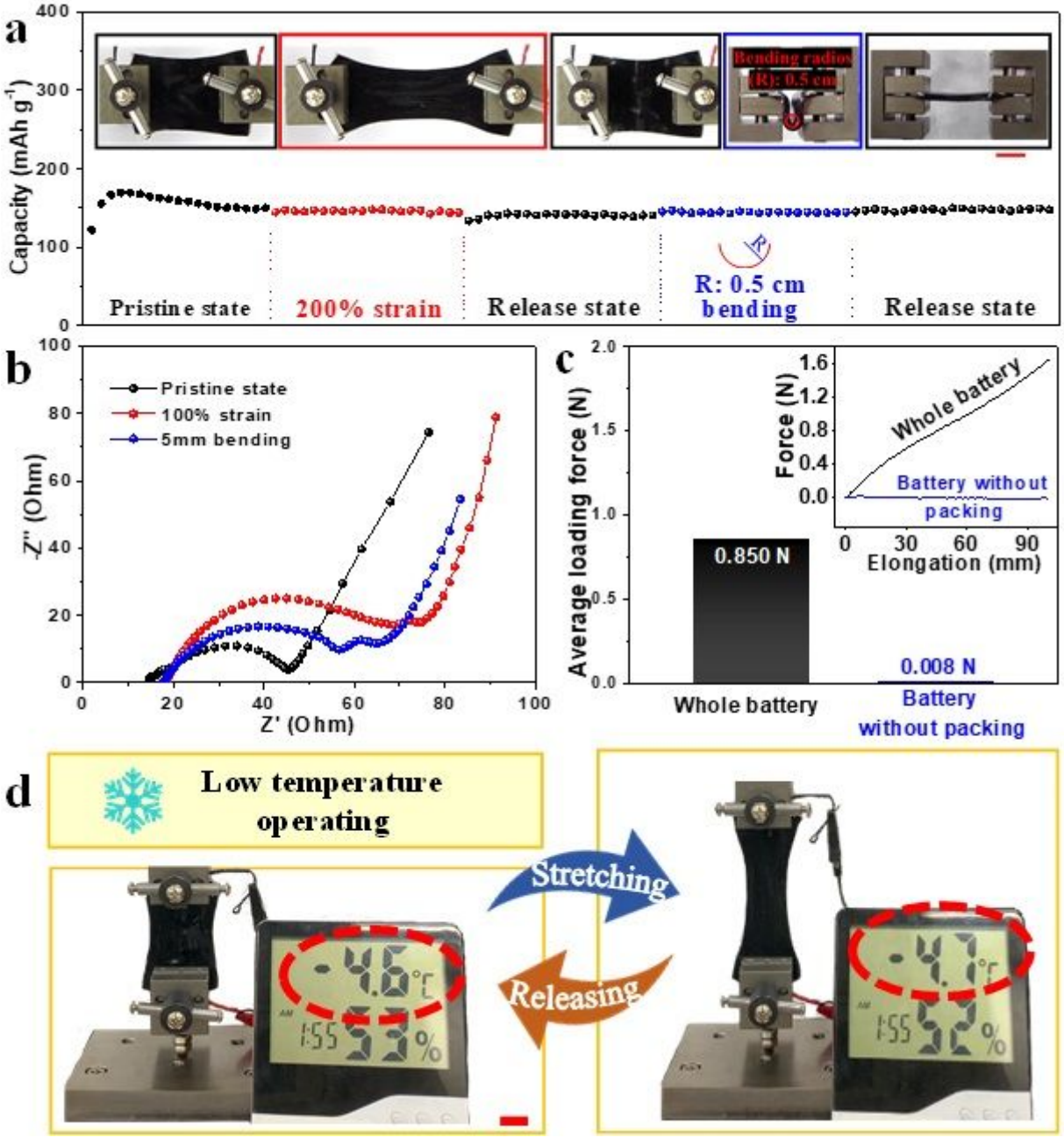

Figure 5

Deformability of the GaInSn–PANI battery with a 2-D structure at room and sub-zero temperatures. a Cycling performance and b Nyquist plots of the battery in stretched, bent, and released states at 25 oC. c Average force and load vs elongation degree plot (inset) of the battery with or without packing at 25 oC. d Photos showing the elasticity of the battery at -4.6 oC. The red scale bars represent 2 cm.

Supplementary Files

This is a list of supplementary files associated with this preprint. Click to download.

- SupplementaryVideo12Dbatterystretching.mp4

- SupplementaryVideo21Dbatterystretching.mp4
- SupplementaryInformation.pdf
- TableofContentsGraphic.pdf